Joule, Volume *9*

Supplemental information

A decade of insights: Delving into calendar aging trends and implications

Vivek N. Lam, Xiaofan Cui, Florian Stroebl, Maitri Uppaluri, Simona Onori, and William C. Chueh

A Decade of Insights: Delving into Calendar Aging Trends and Implications

Vivek Lam[†1,2], Xiaofan Cui[†3], Florian Stroebl[†3], Maitri Uppaluri[3], Simona Onori[⋆3] and William C. Chueh[⋆1,2]

[1]Department of Materials Science and Engineering, Stanford University, Stanford, CA, USA.
[2]Applied Energy Division, SLAC National Accelerator Laboratory, Menlo Park, CA, USA.
[3]Department of Energy Science and Engineering, Stanford University, Stanford, CA, USA.

S.1 Supplemental Notes

S.1.1 Note 1: Derivation for Capacity and Resistance Loss Equations

The capacity relative loss (Q_{rel_loss}) and resistance relative growth (R_{rel_growth}) defined in terms of the capacity and resistance data is given by:

$$Q_{rel\_loss}(t)[\%] = -\frac{Q(t) - Q(0)}{Q(0)} * 100\% \tag{S.1}$$

$$R_{rel\_growth}(t)[\%] = \frac{R(t) - R(0)}{R(0)} * 100\% \tag{S.2}$$

where Q(t) represents the capacity at a given time t, Q(0) is the initial capacity, at t=0, R(t) represents the resistance at time t, and R(0) is the resistance at t=0.

The expression for capacity loss (Q_{rel_loss}(t)), described by the power-law equation, and the relationship between relative capacity loss and relative capacity (Q_{rel}(t)) is given by:

$$Q_{rel\_loss}(t)[\%] = a_Q t^{b_Q} \tag{S.3}$$

[†]These authors contributed equally to this work
[⋆]Corresponding Author. e-mail: wchueh@stanford.edu; sonori@stanford.edu

$$Q_{rel}(t)[\%] = 100\% - Q_{rel\_loss}(t) \tag{S.4}$$

$$Q_{rel}(t)[\%] = 100\% - a_Q t^{b_Q} \tag{S.5}$$

where the exponential b parameter (b_Q or b_R, dimensionless units) captures the time-dependent behavior of degradation and the pre-exponential a parameter (a_Q or a_R, units of $\%/weeks^b$) encodes the rate of degradation.

The expression for resistance growth (R_{rel_growth}(t)), described by the power-law equation, and the relationship between the relative resistance growth and relative resistance (R_{rel}(t)) is given by:

$$R_{rel\_growth}(t)[\%] = a_R t^{b_R} \tag{S.6}$$

$$R_{rel}(t)[\%] = 100\% + R_{rel\_growth}(t) \tag{S.7}$$

$$R_{rel}(t)[\%] = 100\% + a_R t^{b_R} \tag{S.8}$$

The resistance metric defined in Equation 3 can also be seen as an electrode area normalized resistance or the resistivity (where J is the current density) under the assumption that nominal capacity ($Q_{nominal}$) is proportional to the active area that current passes through on the electrode material.

$$R = \frac{\Delta V}{\Delta \text{C-Rate}} = \frac{\Delta V}{\Delta I / Q_{nominal}} \propto \frac{\Delta V}{\Delta I / Area} = \frac{\Delta V}{\Delta J} \tag{S.9}$$

S.1.2 Note 2: Arrhenius-Type Temperature Dependence Extrapolation

The Arrhenius extrapolation show in Figure 2 is justified only under certain constraints on the functional form of degradation. In this section we will go through two examples of when this is justified. In the case where the capacity degradation is fully separable ($Q_{rel\_loss}(T, SOC, t) = A(T) \cdot F(SOC) \cdot G(t)$) and the temperature functional is the Arrhenius equation ($A(T) = a_0 \exp\left(\frac{-E_a}{k_b T}\right)$, by taking the log transform a linear relationship between ln(capacity loss) and ln(1/T) should emerge at fixed SOC and t.

$$\ln(Q_{rel\_loss}(T, SOC, t)) \propto \ln(a_0) - \frac{E_a}{k_b T} + \ln(G(t)) + \ln(F(SOC)) \tag{S.10}$$

Under these conditions there should be a constant activation energy, but as we see in Figure 2 the activation energy is not constant across time. In this case we could allow the temperature functional to

have a time dependence to account for changing activation energy

$$Q_{rel\_loss}(T, SOC, t) = A(T, t) \cdot F(SOC) \cdot G(t) \tag{S.11}$$

$$A(T, t) = a_0(t) \exp\left(\frac{-E_a(t)}{k_b T}\right). \tag{S.12}$$

By refitting this equation at every point in time we can get the Arrhenius predicted curve shown in Figure 2 and SI Figure S4. However, the family of equations this works for can be thought of more generally. Given a slightly different separability assumption ($Q_{rel\_loss}(T, SOC, t) = H(T, SOC, t) \cdot G(t)$), straight lines will be produced for any functional form that satisfies

$$\ln(H(T, SOC, t)) \propto \gamma(t, SOC)\frac{1}{T}.$$

at a fixed temperature and SOC. For example, one common approach is to model the SOC dependence with a Tafel equation

$$F(T, SOC, t) \propto \exp\left(\frac{\alpha z q_e}{k_b}\left(\frac{U_a(SOC, t) - E_{red}}{T}\right)\right)$$

where z is the number of electrons involved in the reaction, q_e is the charge of an electron, $U_a(SOC, t)$ is the anode potential, and E_{red} is the reduction potential of the electrolyte. If we define $H(T, SOC, t) = A(T, t) \cdot F(T, SOC, t)$, this function follows Equation S.1.2 so this would still produce straight lines in the Arrhenius plot at a given SOC and time. Examples of functional forms that would not work are T, T^2, $\exp(\frac{1}{T^2})$, etc.

S.1.3 Note 3: Activation Energy Semi-Empirical Fitting Method

The activation energies and the corresponding confidence intervals are extracted by taking the a values, transforming them in to log space and then performing a weighted least squares linear regression using the statsmodels python package. The weights of each sample are proportional to the inverse of the number of samples at a temperature, weighing the total data at each temperature equally. The extracted slope is then converted to the activation energy and the corresponding 90% confidence interval is plotted in Figure 4. The 85°C data points are excluded from the weighted least squares fitting due to the presence of additional degradation modes, as well as for better comparison of all cells within their nominal operating temperature regime. The mean log a values are plotted for relative capacity and relative resistance in SI Figure S5 for all cell types with two or more temperature data points that have non-zero a values. The

replicates and activation energy line of best fit extraction are shown in SI Figure S6 and S7 for relative capacity and relative resistance respectively.

In this process, the influence of fitting uncertainty in the semi-empirical power law is not accounted for. In particular, this is important for very gradual degradation cases where the a value is very close to 0 (as seen for K2 Energy LFP18650E and Tenergy 302030 cells in Section **??**). When the log transform is taken this can exacerbate these pertubations close to 0 leading to large variability as can be seen in SI Figure S7 for K2 Energy LFP18650E and Tenergy 302030 cells. Additionally, in these cases the fitting of the b parameter can increase in uncertainty. This is implicitly seen through the large variability of fitting on repeats for K2 Energy LFP18650E and Tenergy 302030 cells in Figure 5. In this work, the variability induced due to fitting error is not further accounted for.

S.1.4 Note 4: Literature Review Table

Table S3 reproduced at the bottom of the SI document summarizes the cell type, testing conditions, testing duration and state of health (SOH) reached at end of testing (EOT) taken from literature. Studies with commercial cells, unique testing conditions, and longer testing durations were preferentially included. The data is extracted predominantly using a webplot digitizer, the values reported are approximate. The data of these testing conditions versus our work is shown in SI Fig S1,S2.

S.2 Supplemental Figures

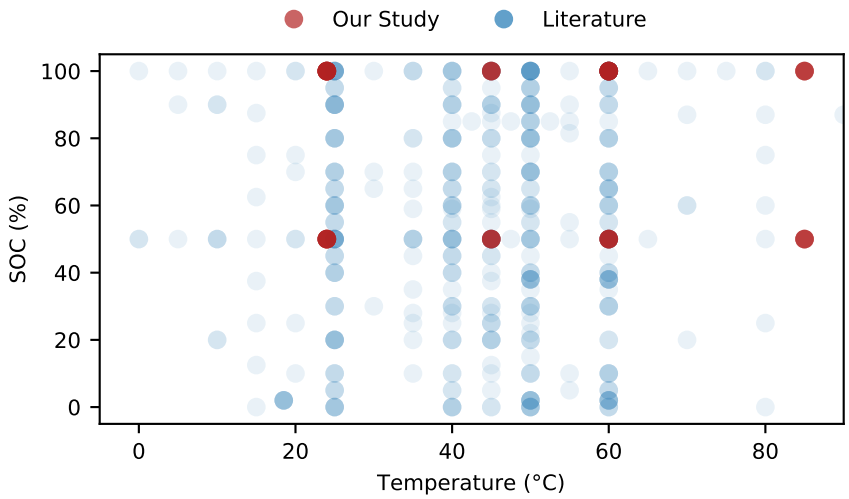

Fig. S1: **Literature testing conditions**. Testing conditions of a representative subset of calendar aging literature with the testing condition of our study overlaid. For a table of these values see SI Section S.1.4.

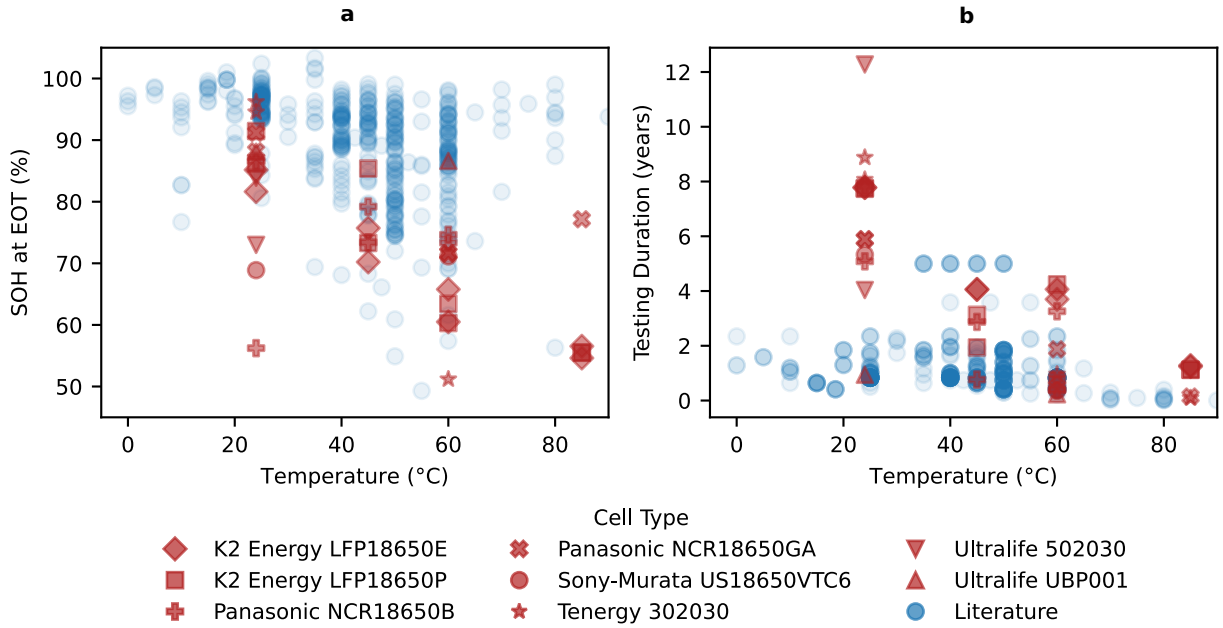

Fig. S2: **Literature testing duration**. A representative subset of the duration of calendar aging studies is shown through **a)** state of health (SOH) at end of testing (EOT) and **b)** testing duration in years. Lower temperature aging for long durations and lower SOH is lacking. To see table of values taken from literature data see SI Section S.1.4.

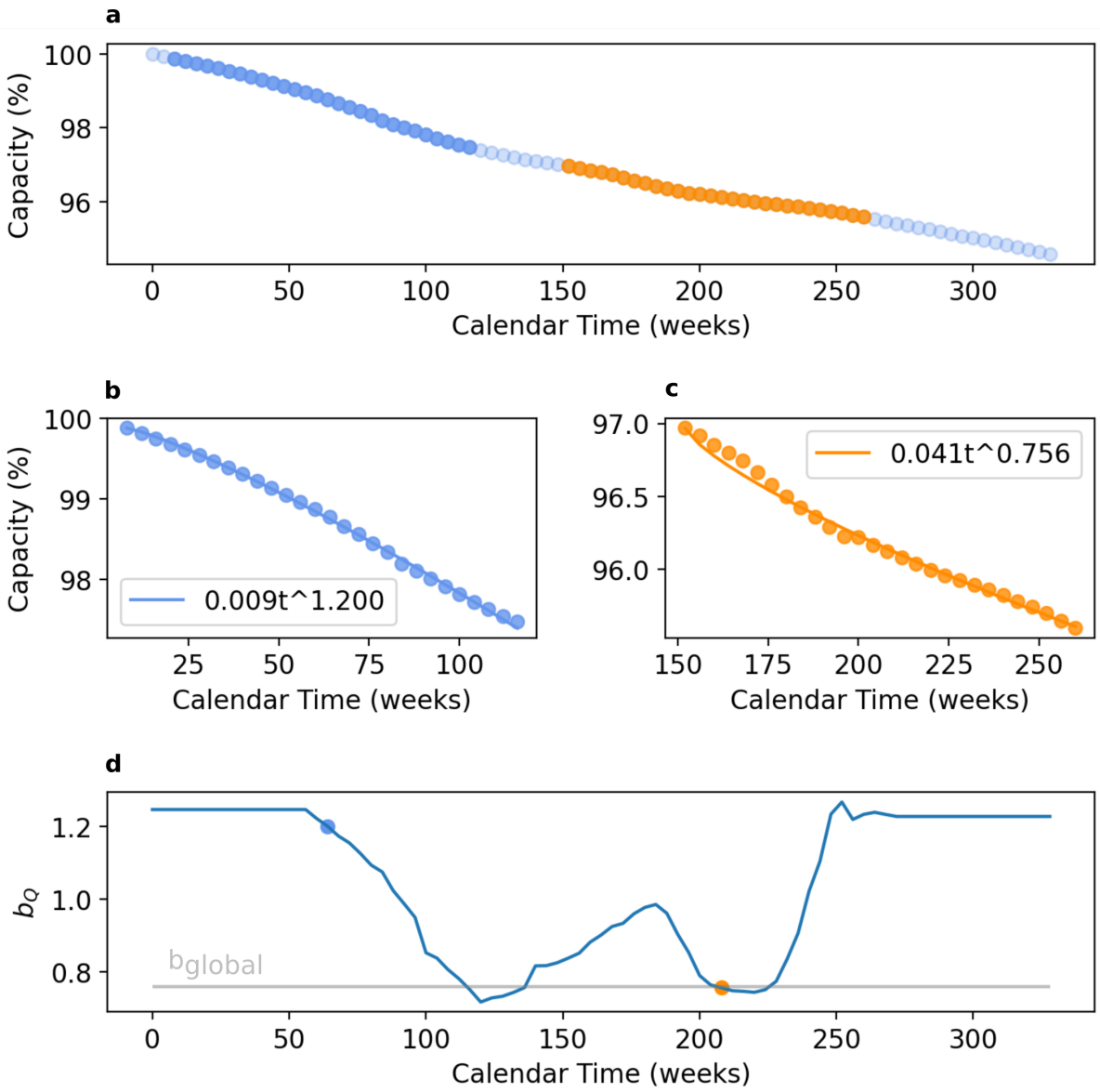

Fig. S3: **Time dependent non-linearity of capacity degradation.** Local time model fitting vs global time model fitting for power law equations ($a_Q t^{b_Q}$) can yield very different results due to the time dependent non-linearities of the system. **a)** Curve showing the normalized capacity degradation of a Tenergy 302030 battery at 100% SOC and 24C. The blue and orange regions are example regions spanning 1/3 of the data where the fit will be highlighted. **b)** Fitting a power law based model on the blue region showing accelerating degradation. **c)** Fitting a power law model on orange region showing decelerating degradation. **d)** Plot showing how the capacity exponential parameter b_Q changes over the course of degradation fit on a moving window of 1/3 of the data . The example regions in **b)** and **c)** are shown as a blue and orange point respectively. The global fit of the exponential parameter is shown with a gray horizontal line. This demonstrates how looking at small segments of the data may give incorrect extrapolations highlighting the challenges involved in modeling this behavior.

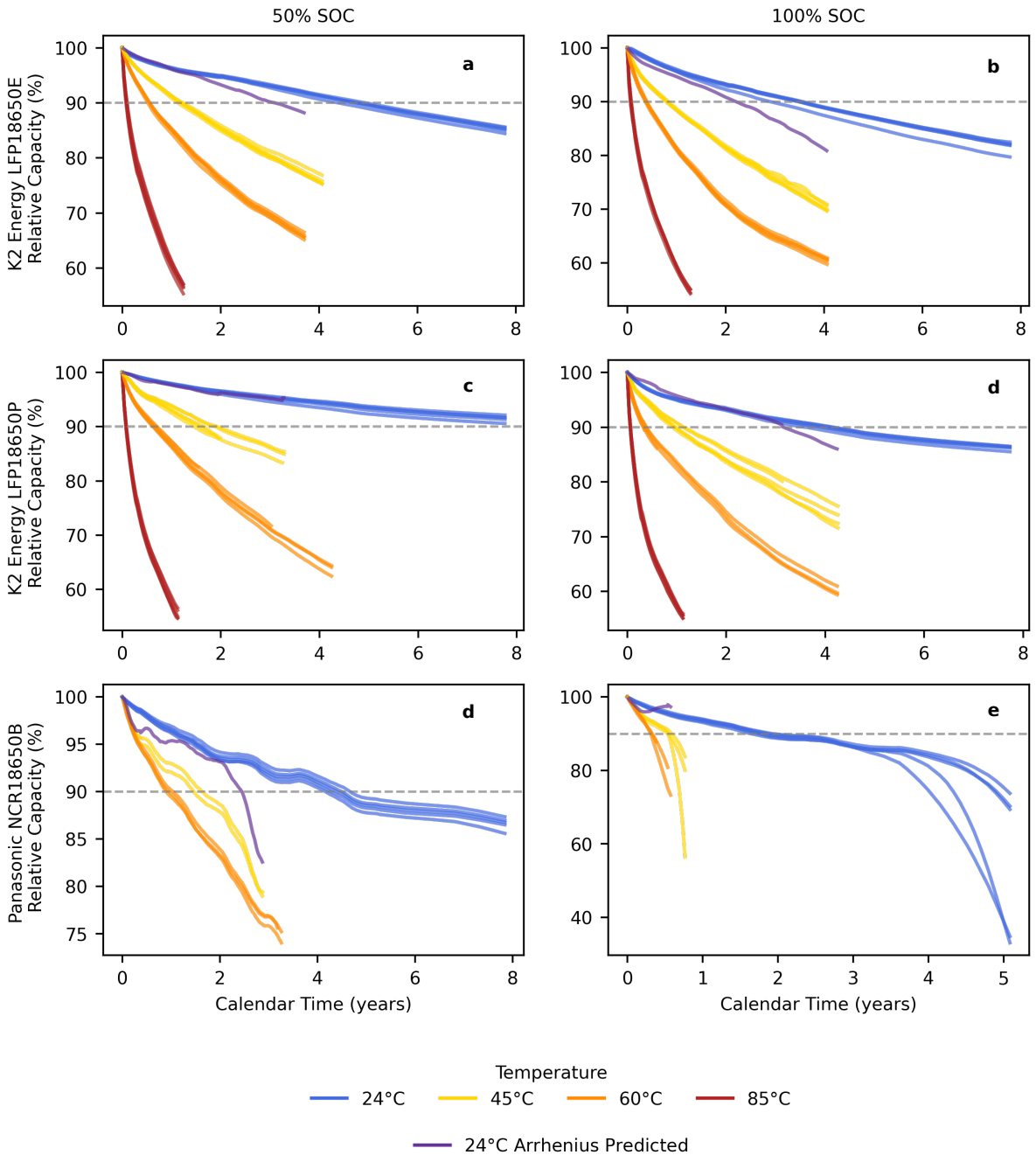

Fig. S4: **Arrhenius predicted 24°C degradation curves**. Arrhenius extrapolated 24°C degradation curves shown in Figure 2. In these plots, the 45°C and 60°C data is shown so that the origin of the trends of the Arrhenius 24°C are clear. Although the 85°C data is shown here for reference, it is not used in the analysis due to the short lived nature of this testing condition. These curves are shown for both 50% and 100% for **a,b)** K2 Energy LFP18650E, **c,d)** K2 Energy LFP18650P, and **e,f)** Panasonic NCR18650B. These cell types are chosen as they are the ones in the dataset present with 24°C, 45°C, and 60°C data.

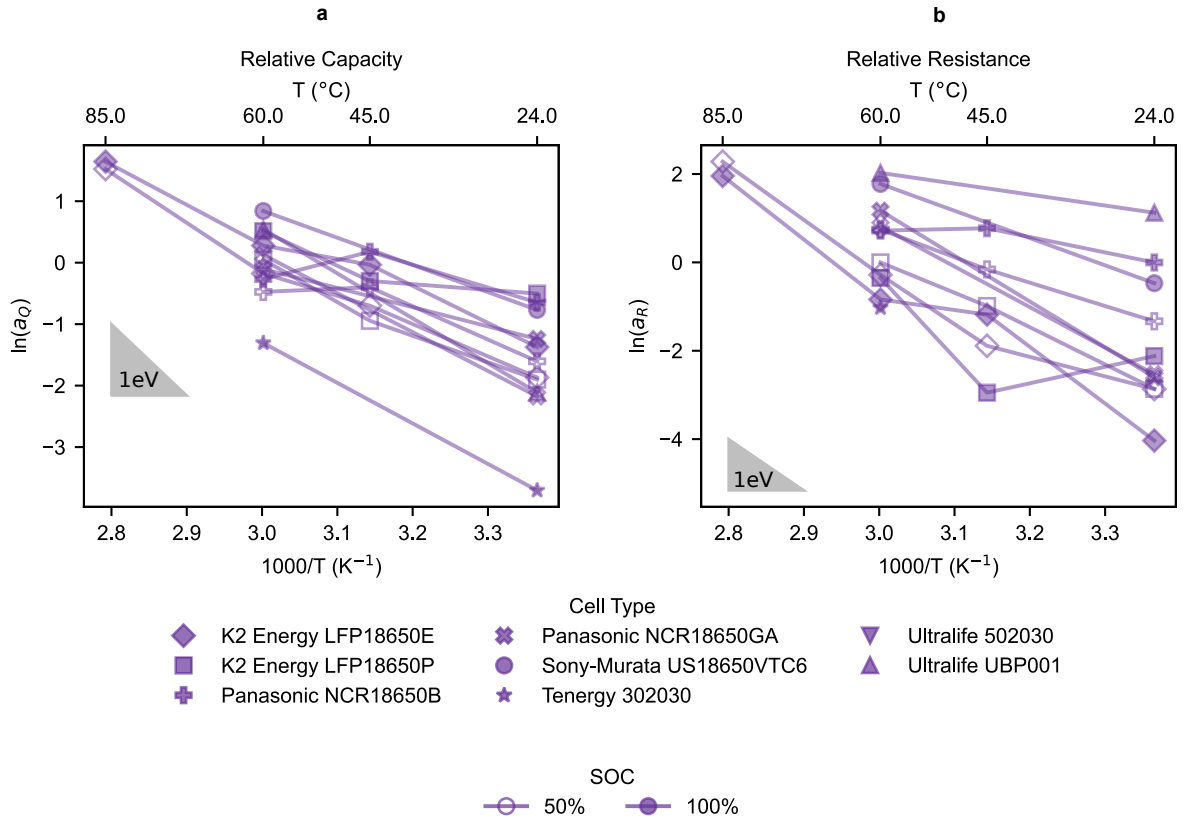

Fig. S5: **Arrhenius plot of power law pre-exponential factor**. Arrhenius plot of mean log **a)** a_Q and **b)** a_R values including cell types with only two unique temperatures. To see the individual cell repeats and activation energy extraction see SI Figure S6 for relative capacity and SI Figure S7 for relative resistance.

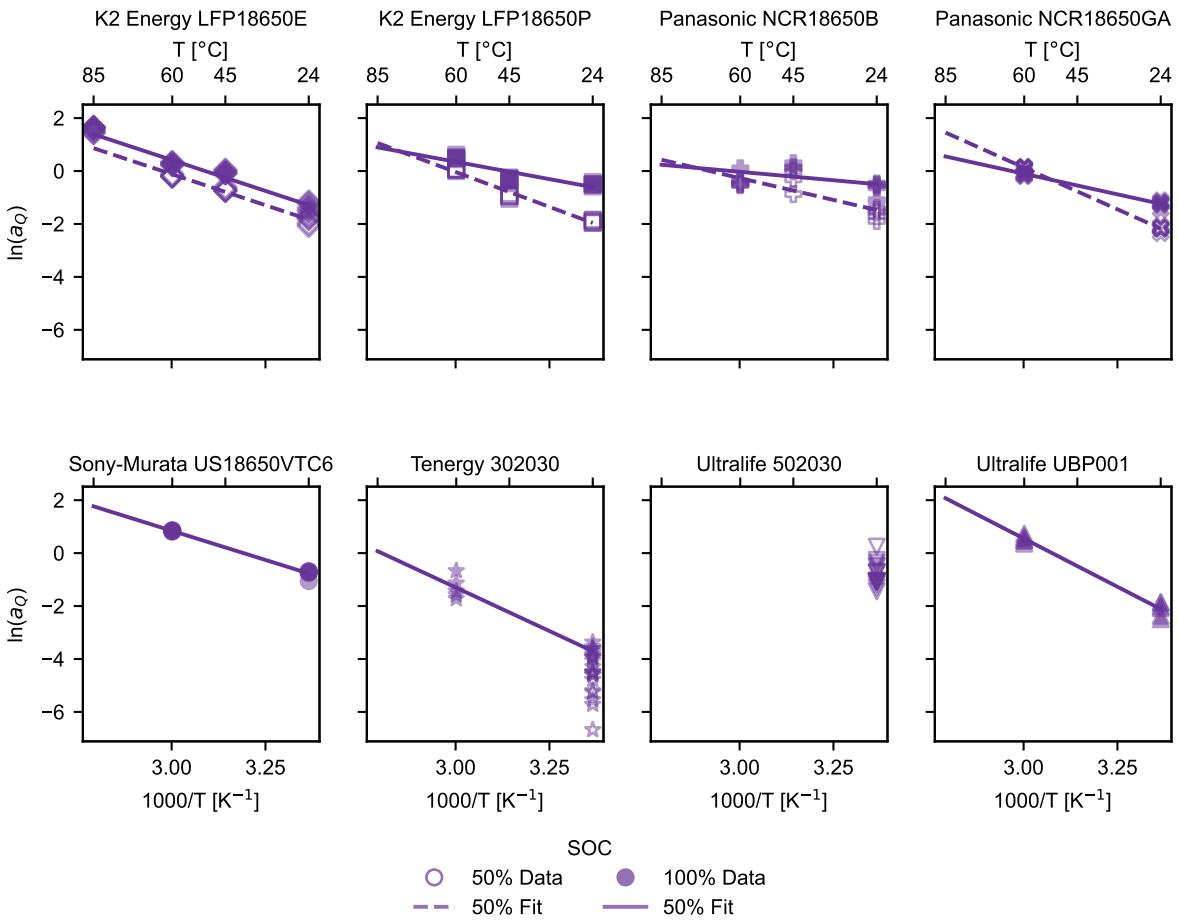

Fig. S6: **Individual cell type capacity activation energy extraction**. Extraction of activation energy slope from the relative capacity a_Q for each cell type. Markers show the data points and the line is the weighted least squares line of fit weighing each temperature 60°C and lower equally.

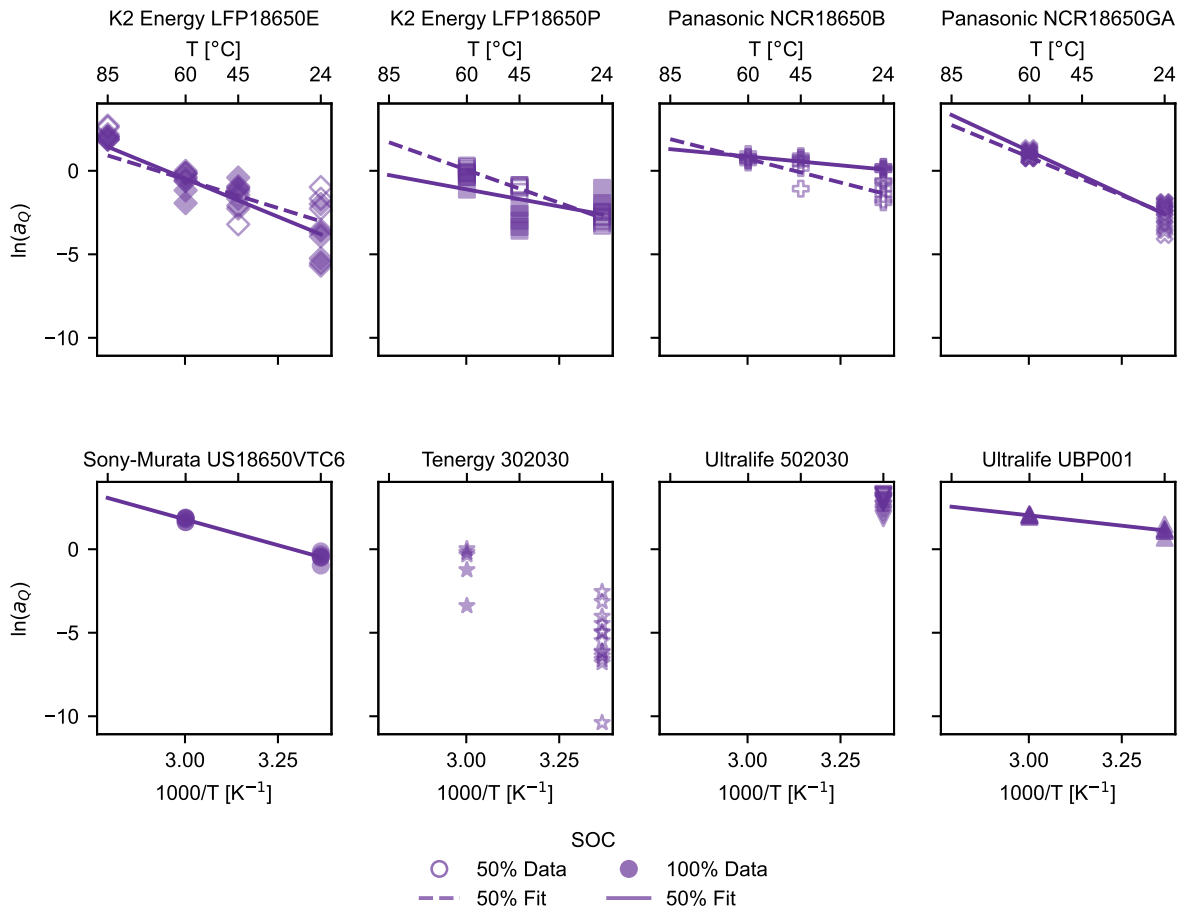

Fig. S7: **Individual cell type resistance activation energy extraction**. Extraction of activation energy slope from relative resistance a_R from each cell type. Markers show the data and the line is the weighted least squares line of fit weighing each temperature 60°C and lower equally. Tenergy 302030 cells were unable to be extracted as 24°C a_R values are very close to 0 making it undefined in log space.

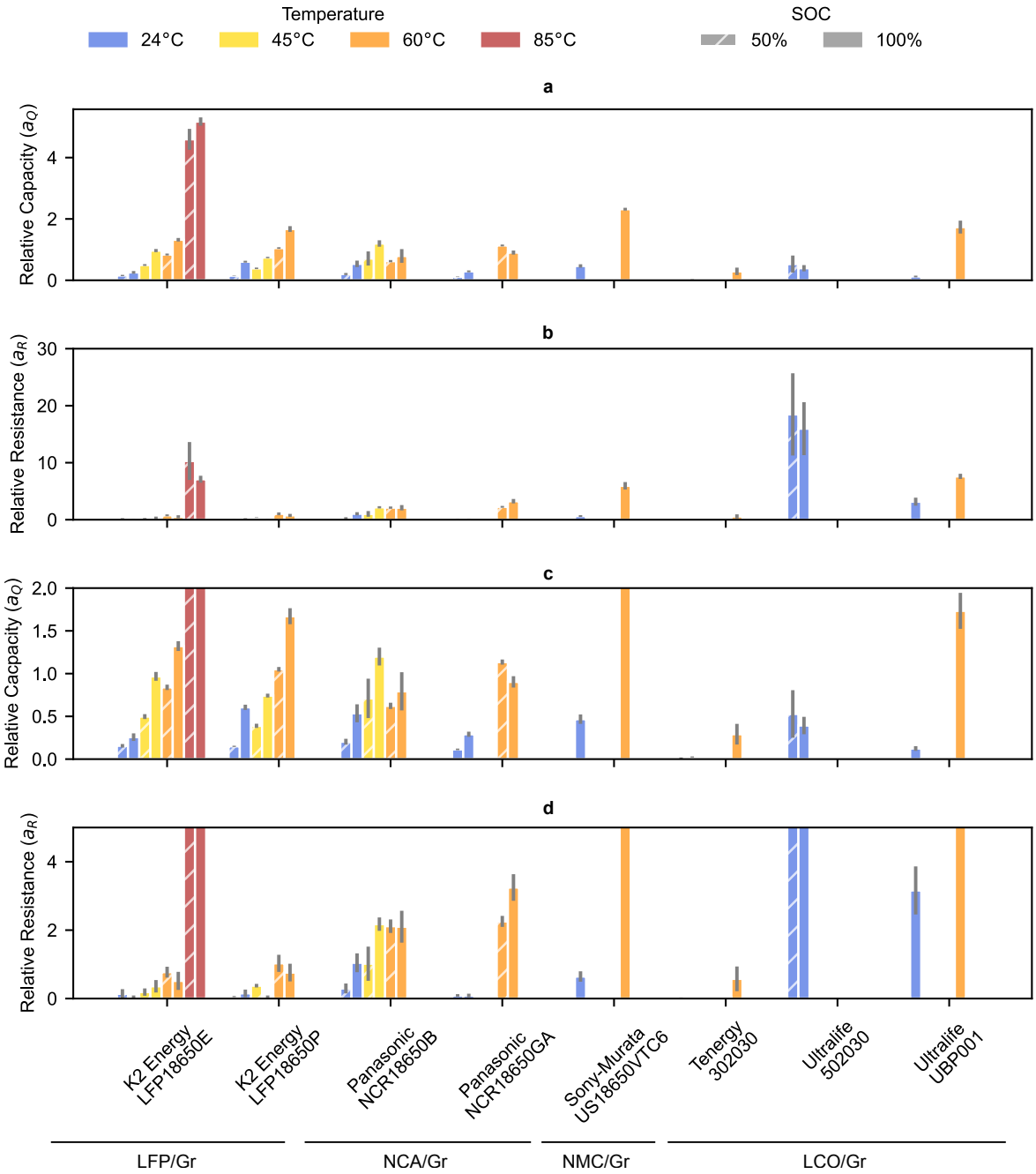

Fig. S8: **Pre-exponential parameter dependence on temperature**. Bar plots of the pre-exponential parameter for **a**) relative capacity, and **b**) relative resistance. As some values of the preexponential parameter are quite large, to show the trend more clearly the y-axis is limited to 0 to 2 for **c**) relative capacity, and limited to 0 to 5 for **d**) relative resistance.

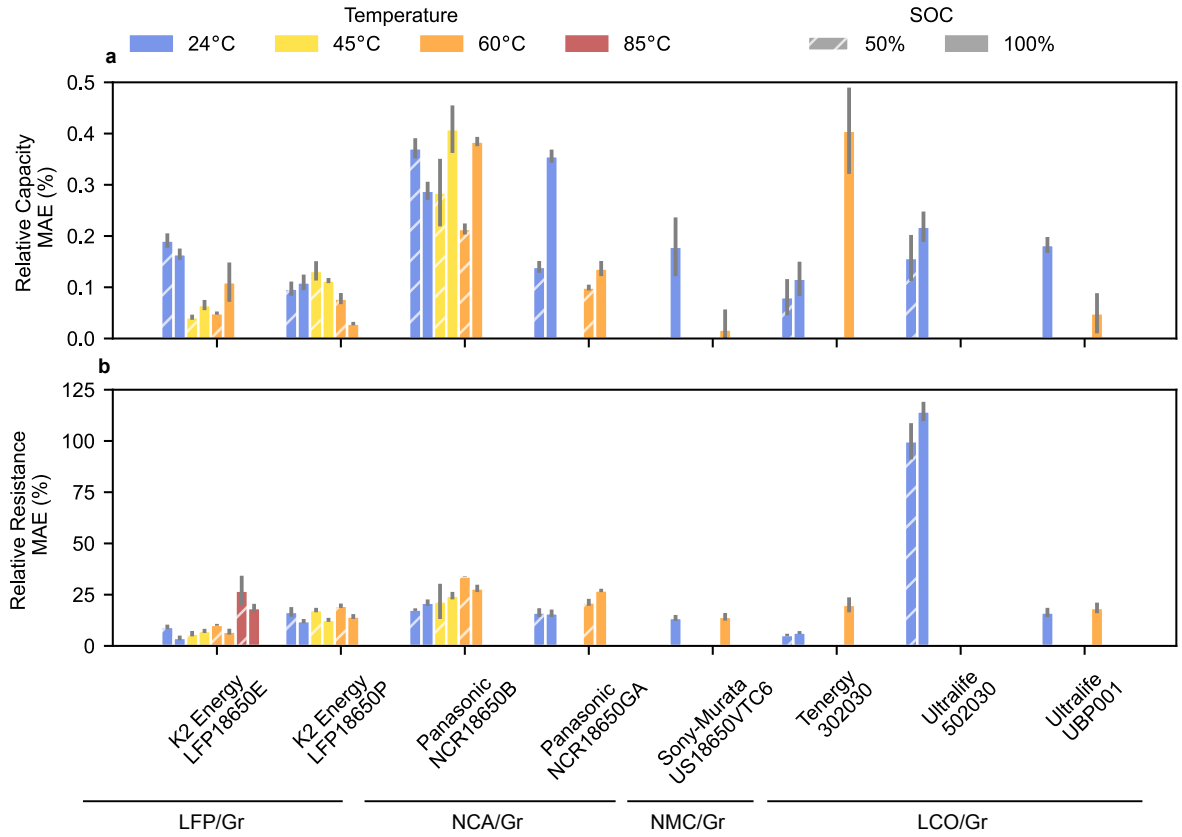

Fig. S9: **Mean absolute error of fitting results**. Bar plots of the MAE for **a**) capacity, and **b**) resistance. As the fit uses relative metrics (Q_{rel} and R_{rel}) the MAE has units of percent, but this is not to be confused with mean absolute percent error (MAPE).

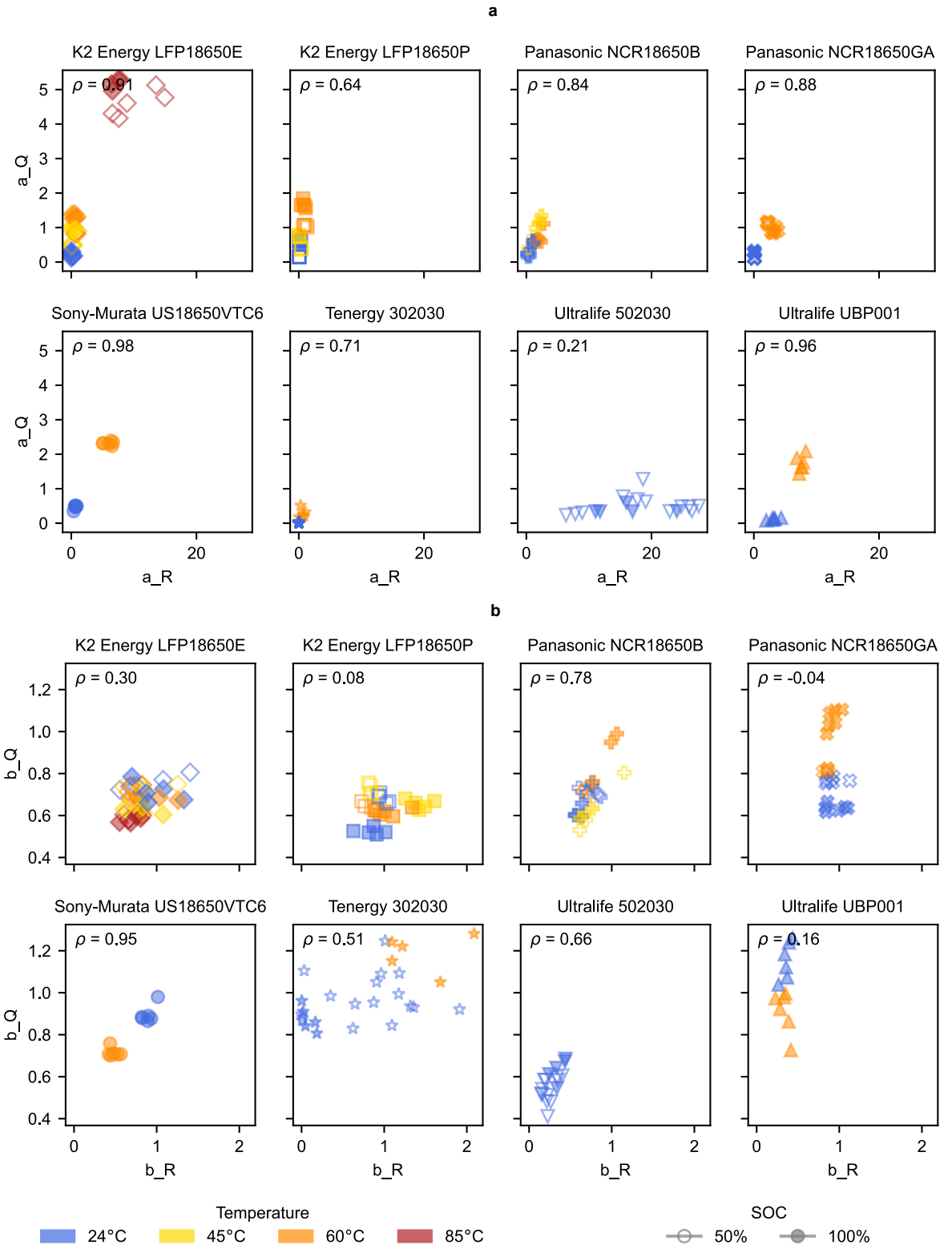

Fig. S10: a_Q **vs.** a_R **and** b_Q **vs.** b_R **parameter correlation per cell type**. **a)** The a_Q and a_R values are compared for each cell type individually. **b)** The b_Q and b_R values are compared for each cell type individually. The pearson correlation is presented in the top left of each plot. While a general correlation is observed for almost all cell types in the case of the a parameter, no clear correlation is observed for the majority of cell types for the b parameter. A good b parameter correlation exists for Panasonic NCR18650B cells and Sony-Murata US18650VTC6 cells, but this does not seem to generalize to similar chemistry indicating deeper characterization is critical in separating our degradation behavior trends.

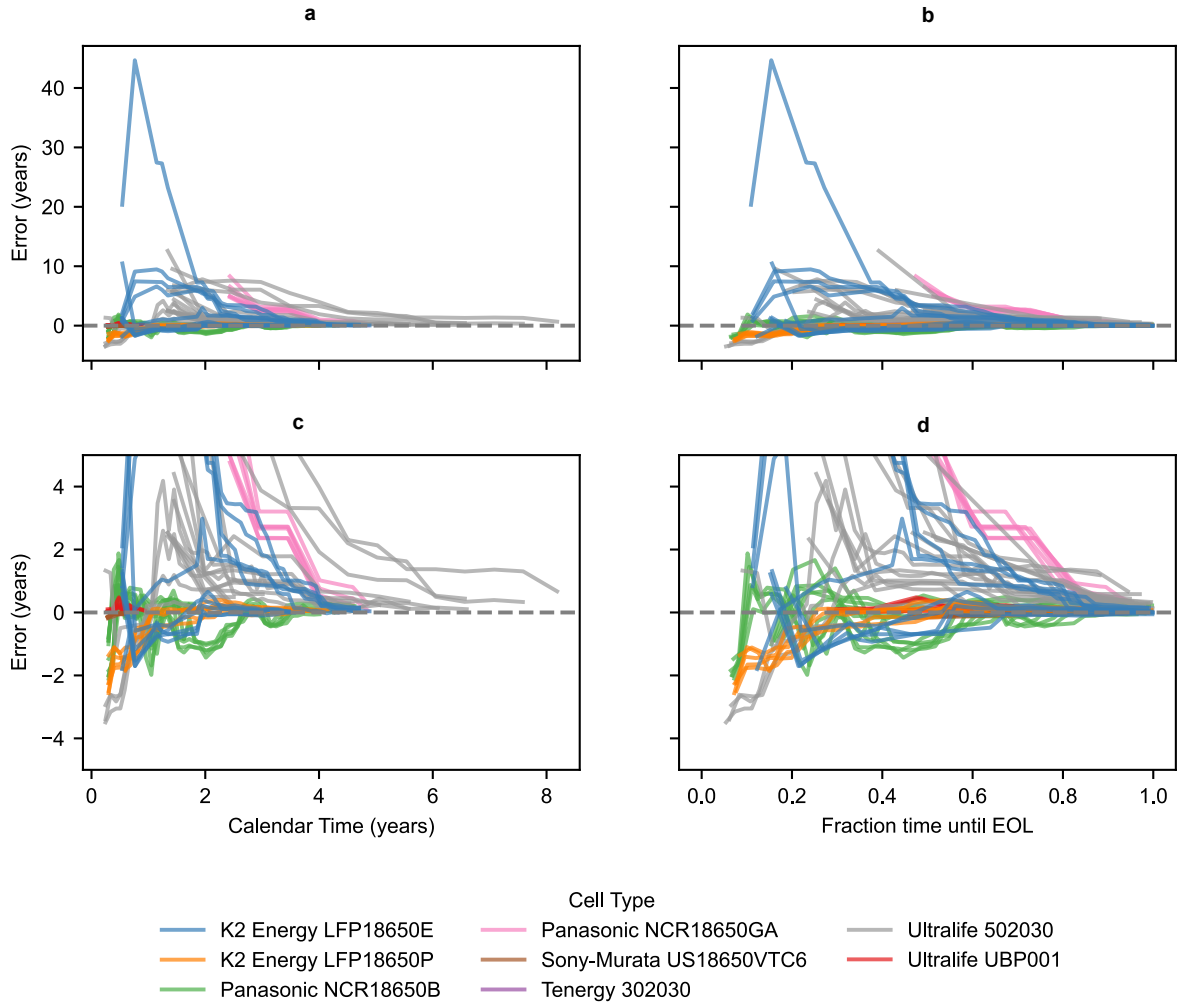

Fig. S11: **Power-law cell type EOL error trajectory**. The error trajectories shown in Figure 8b,c are shown here separated by color based on cell type. The full error trajectories are shown against **a)** calendar time in years, and **b)** fraction of time until EOL. To better see the trajectories, the same plots are shown with a y-axis limited between ± 5 years for **c)** calendar time in years, and **d)** fraction of time until EOL. Cell types shown in the legend but not visible on the plot are cell types that have no data that has reached the EOL condition within the testing time(namely the Tenergy 302030 and Sony-Murata US18650VTC6). A dashed gray line is shown at zero error for all plots for reference.

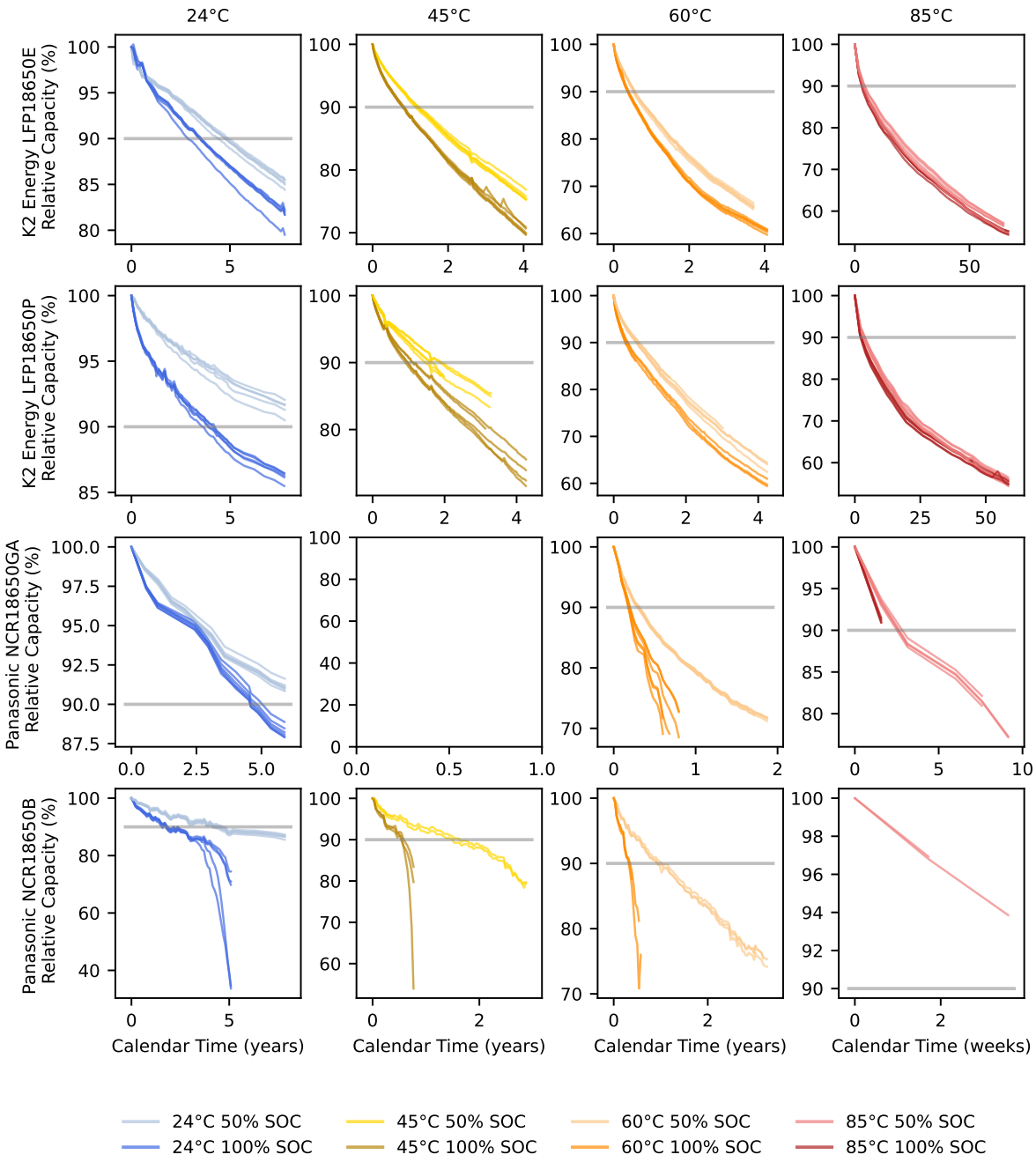

Fig. S12: **Relative capacity trends for all cells part A**. All available data is plotted with different x and y scales to better show trends. The 24, 45, and 60 °C are plotted in years, but the 85 °C data is plotted in weeks due to its short-lived nature. A gray line is shown at the 90% relative capacity EOL point

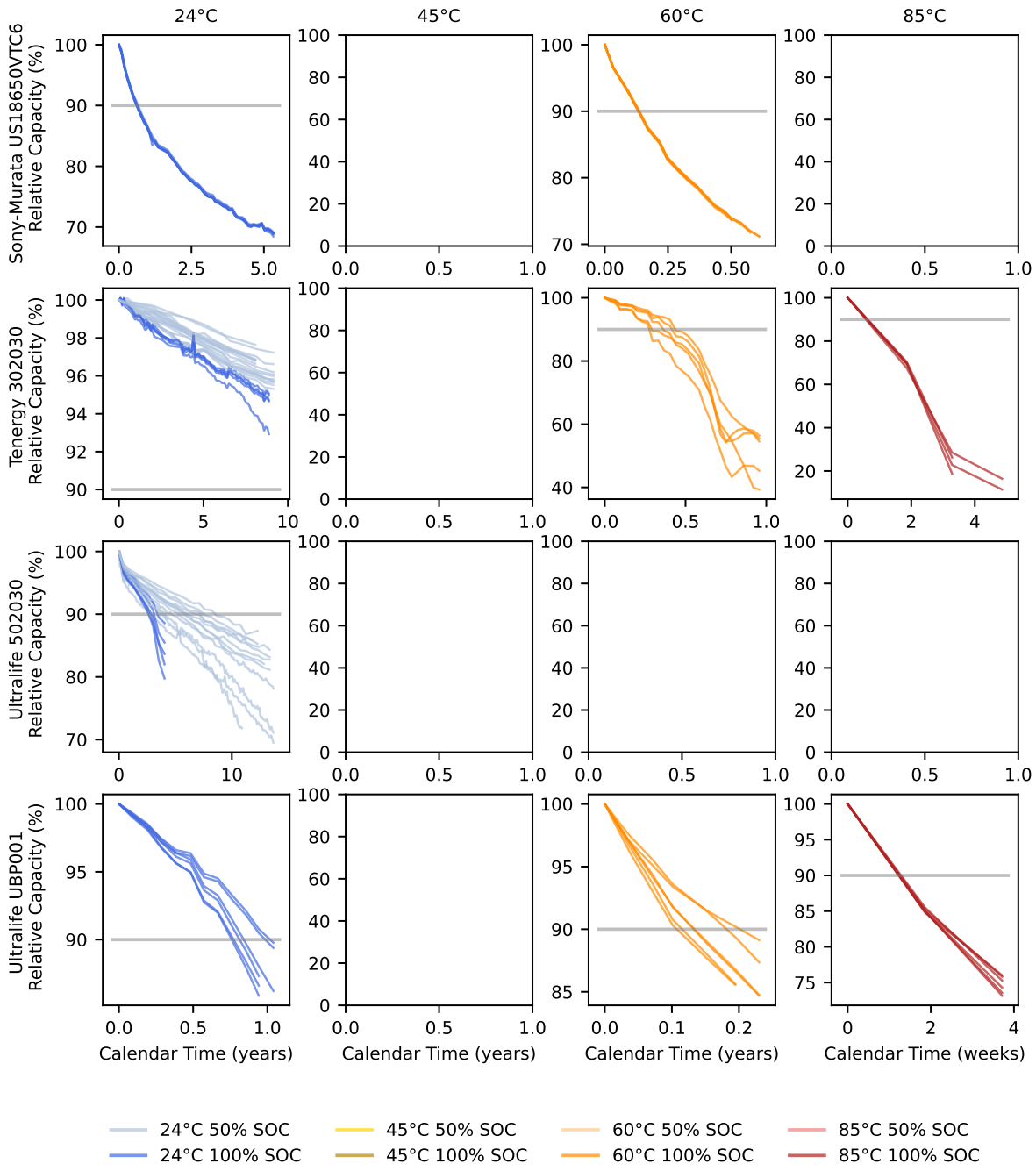

Fig. S13: **Relative capacity trends for all cells part B**. All available data is plotted with different x and y scales to better show trends. The 24, 45, and 60 °C are plotted in years, but the 85 °C data is plotted in weeks due to its short-lived nature. A gray line is shown at the 90% relative capacity EOL point.

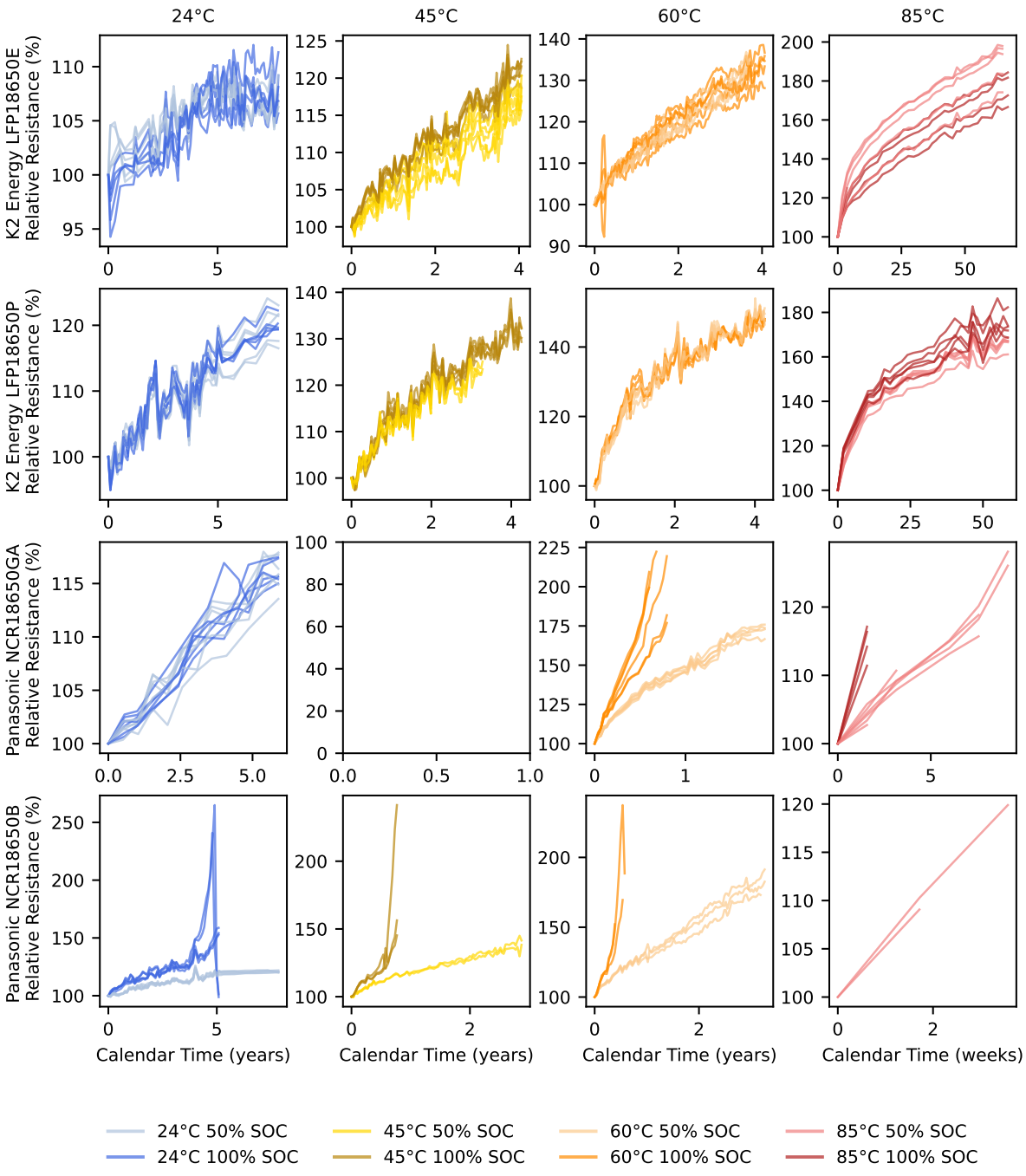

Fig. S14: **Relative resistance trends for all cells part A**. All available data is plotted with different x and y scales to better show trends. The 24, 45, and 60 °C are plotted in years, but the 85 °C data is plotted in weeks due to its short-lived nature.

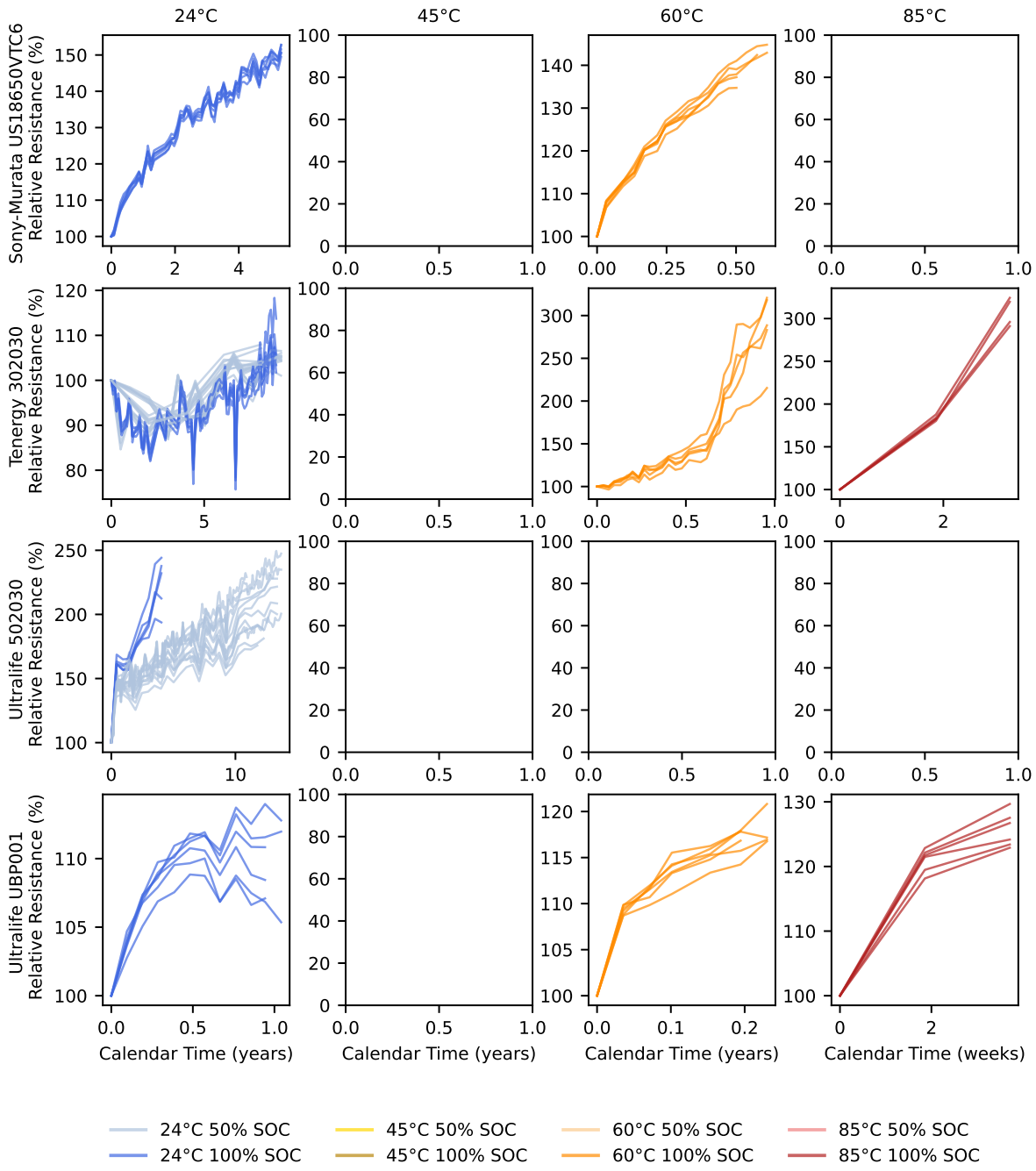

Fig. S15: **Relative resistance trends for all cells part B**. All available data is plotted with different x and y scales to better show trends. The 24, 45, and 60 °C are plotted in years, but the 85 °C data is plotted in weeks.

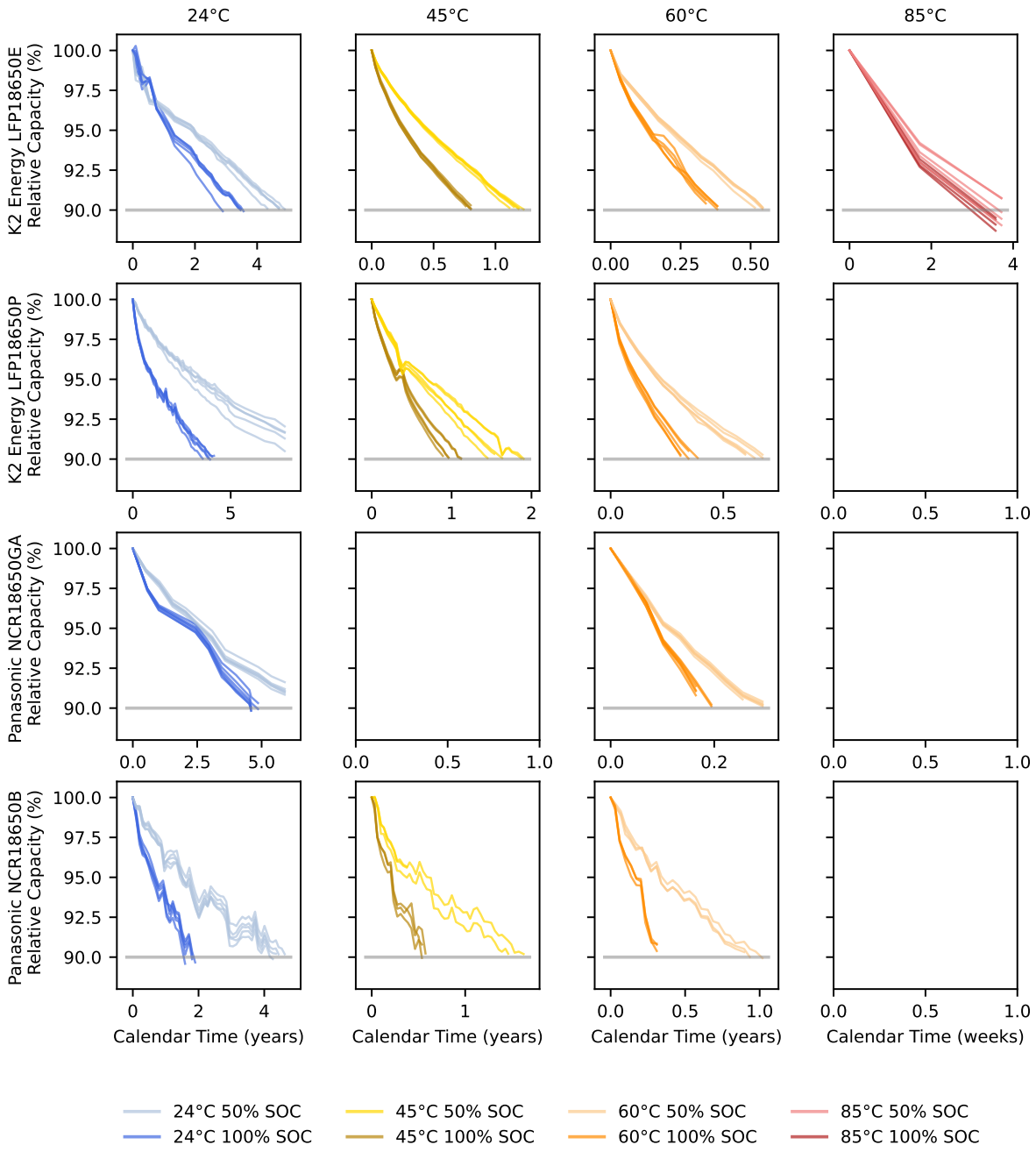

Fig. S16: **Relative capacity trends to 90% capacity part A**. The 90% EOL time is determined by smoothing on all available capacity data for a given cell. Only capacity datapoints less than the EOL time are plotted. This data is what is used to fit the pre-exponential and exponential parameters in the power-law equations.

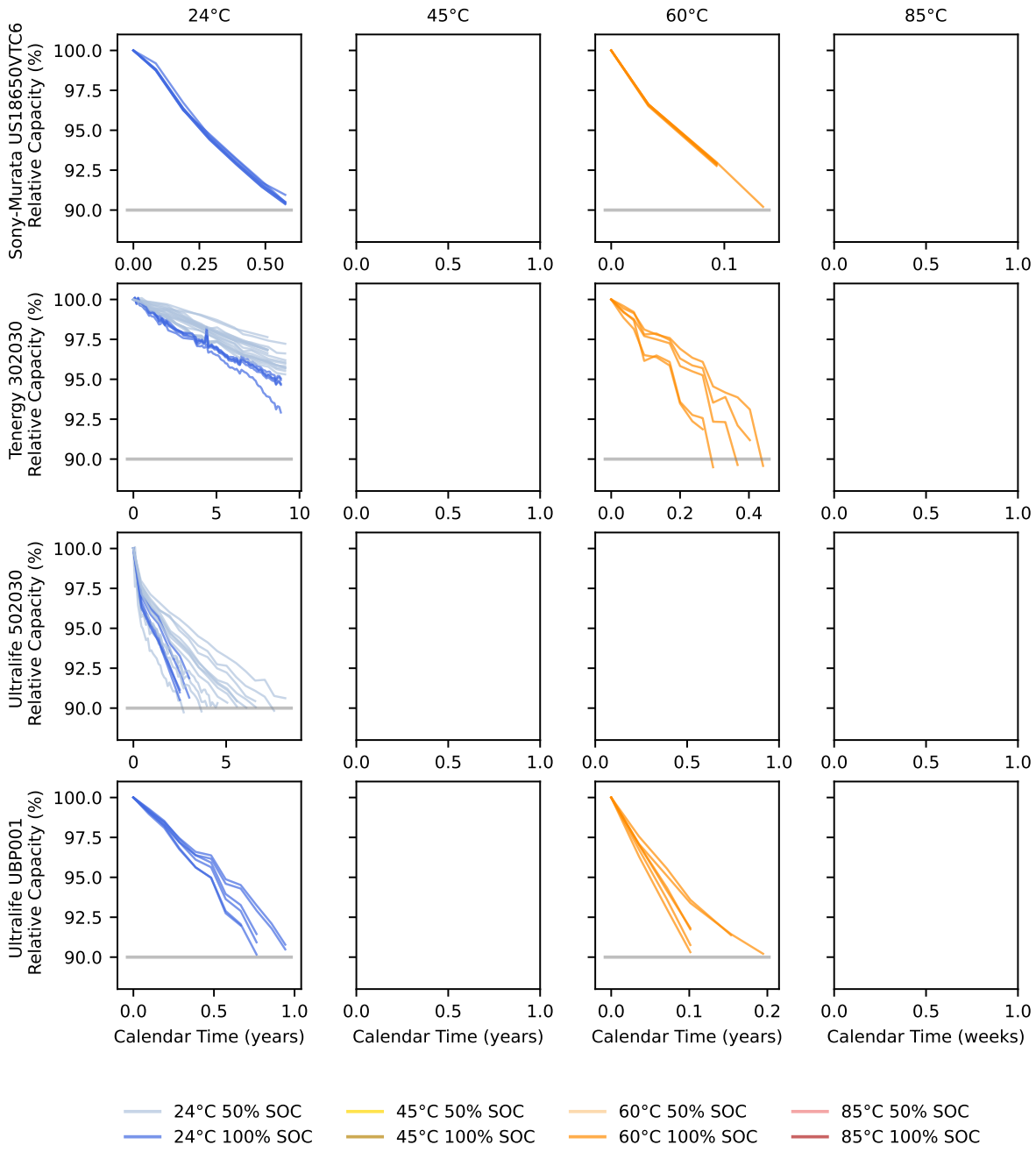

Fig. S17: **Relative capacity trends to 90% capacity b**. The 90% capacity EOL time is determined by smoothing on all available capacity data. Only capacity datapoints less than the EOL time are plotted. This data is what is used to fit the pre-exponential and exponential parameters in the power-law equations.

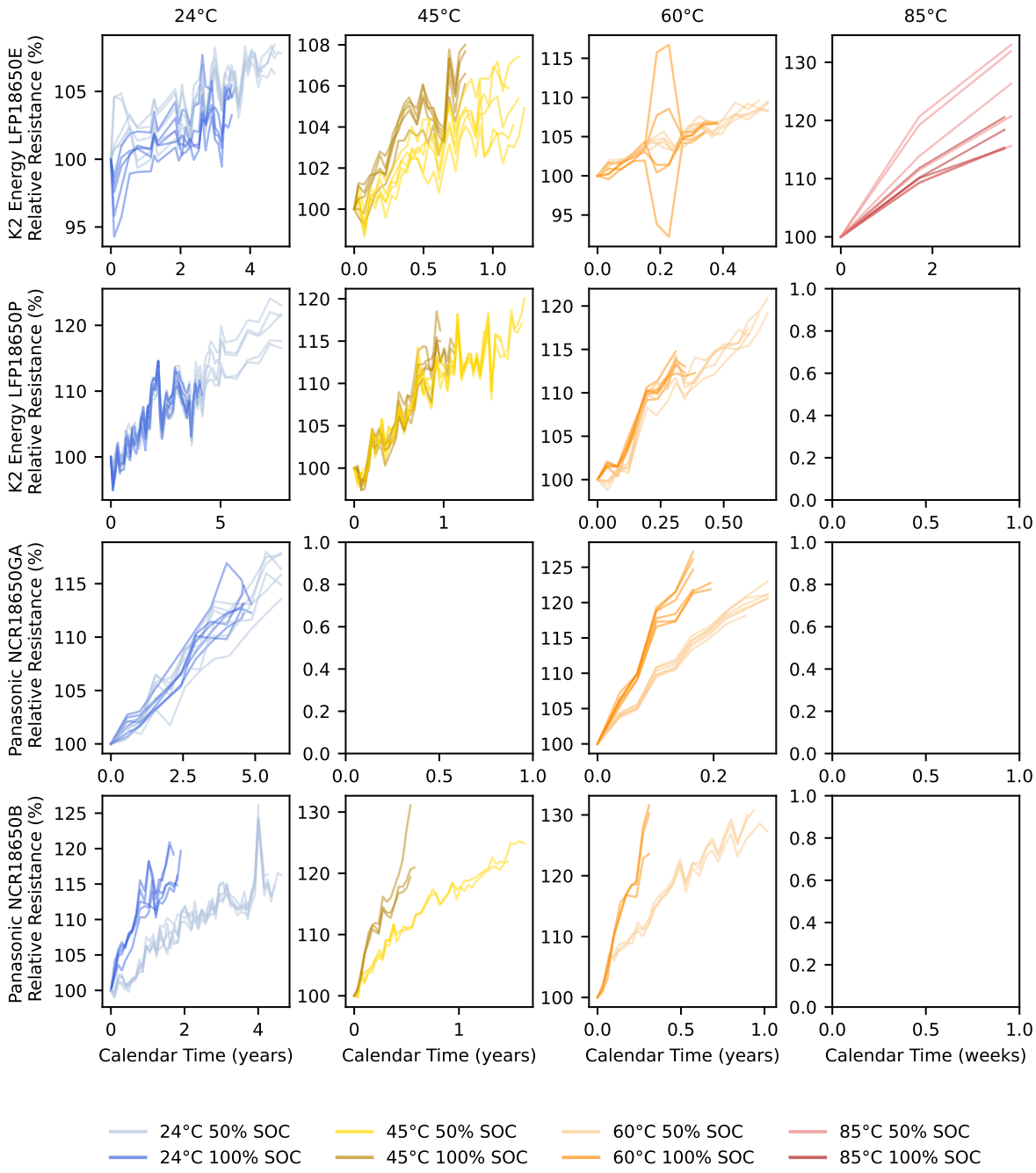

Fig. S18: **Individual relative resistance trends to 90% capacity a**. The 90% capacity EOL time is determined by smoothing on all available capacity data. Only resistance datapoints less than the EOL time are plotted. This data is what is used to fit the pre-exponential and exponential parameters in the power-law equations.

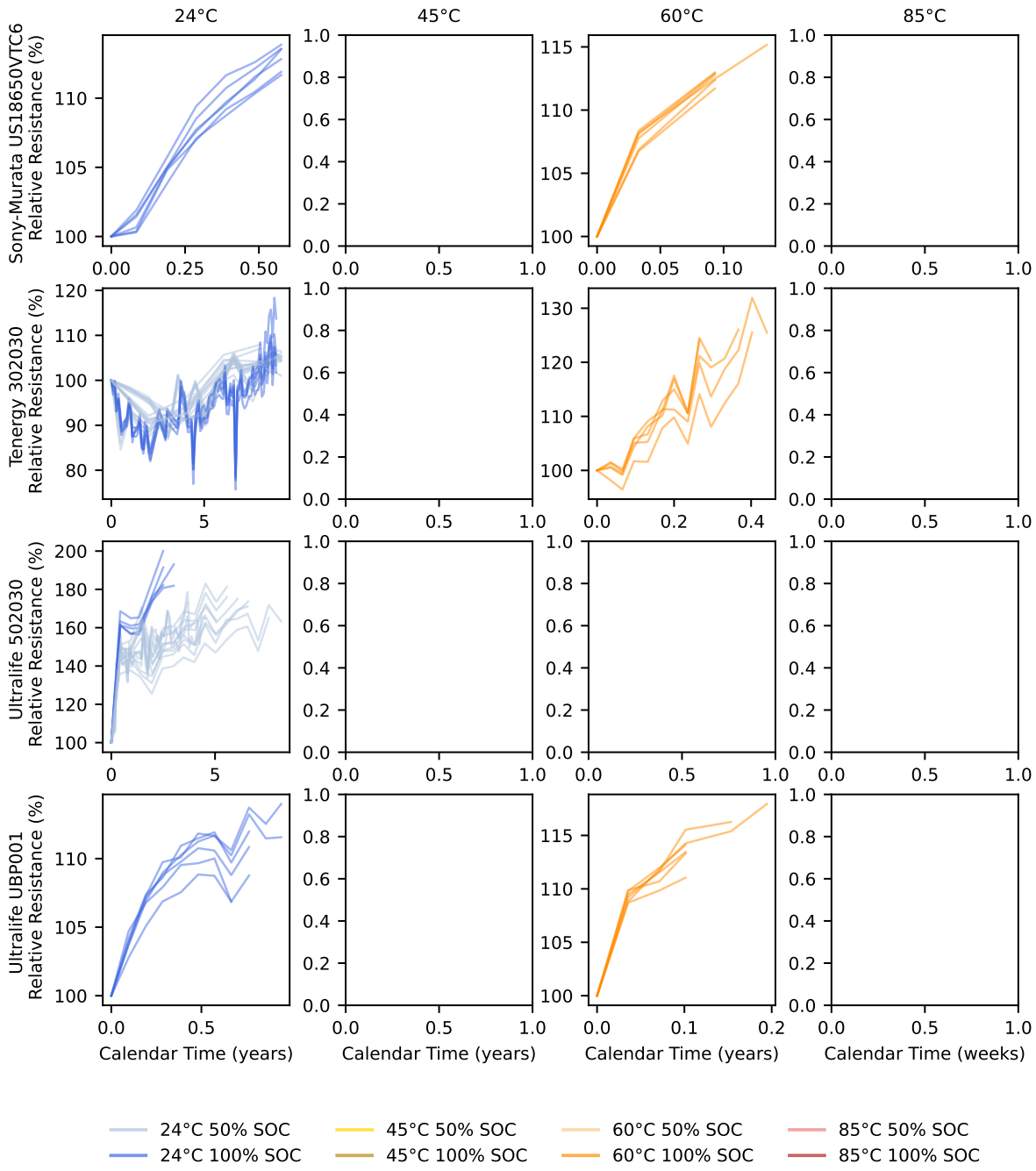

Fig. S19: **Individual relative resistance trends to 90% capacity b**. The 90% capacity EOL time is determined by smoothing on all available capacity data. Only resistance datapoints less than the EOL time are plotted. This data is what is used to fit the pre-exponential and exponential parameters in the power-law equations.

S.3 SI Tables

Step	Type	Value	Limit	End Condition
1	Rest			t = 2min
2	Discharge CC	I = C/5		V ≤ V_{lower}
3	Rest			t = 1hr
Three C/5 Low Rate Cycles				
4	Charge CCCV	I = C/5	V ≤ V_{upper}	I ≤ C/20
5	Rest			t = 1hr
6	Discharge CC	I = C/5		V ≤ V_{lower}
7	Rest			t = 1hr
	Loop to Step 4 two additional times			
Three High Rate Cycles				
8	Charge CCCV	I = C/5	V ≤ V_{upper}	I ≤ C/20
9	Rest			t = 1hr
10	Discharge CC	I = $C_{highrate}$		V ≤ V_{lower}
11	Rest			t = 1hr
	Loop to Step 8 two additional times			
Capacity Check				
12	Charge CCCV	I = C/5	V ≤ V_{upper}	I ≤ C/20
13	Rest			t = 1hr
14	Discharge CC	I = C/5		V ≤ V_{lower}
15	Rest			t = 1hr
Charge for Storage				
		if 100% SOC		
16	Charge CCCV	I = C/5	V ≤ V_{upper}	I ≤ C/20
		if 50% SOC		
16	Charge CC	I = C/5		$Q_{charge} \geq 0.5 \cdot Q_{nominal}$

Table S1: **Diagnostic cycle protocol.** This table shows the nominal diagnostic cycle used to probe the batteries in the dataset. It consists of three low-rate (C/5) cycles, three high-rate (1C, 2C or 3C) cycles, a capacity check, and a charge for storage. In this protocol, the discharge current is negative, while the charge current is positive. The C-rate (1/hr) is defined as the rate at which the battery is charged relative to the nominal capacity ($Q_{nominal}$. For details of the upper voltage cutoff (V_{upper}), lower voltage cutoff (V_{lower}), high C-rate ($C_{highrate}$) and nominal capacity ($Q_{nominal}$) see SI Table S2.

Manufacturer	Cell Name	Nominal Capacity ($Q_{nominal}$)	High Rate C-Rate ($C_{highrate}$)	Low Voltage Cutoff (V_{lower})	High Voltage Cutoff (V_{upper})
K2 Energy	LFP18650E	1.50Ah	3C	2.00V	3.60V
K2 Energy	LFP18650P	1.10Ah*	3C	2.00V	3.65V
Panasonic	NCR18650B	3.30Ah	1C	2.70V	4.20V
Panasonic	NCR18650GA	3.50Ah	1C	2.50V	4.20V
Sony-Murata	US18650VTC6	3.00Ah	3C	2.50V	4.20V
Tenergy	302030	0.12Ah	1C	3.00V	4.20V
Ultralife	502030	0.24Ah	2C	2.80V	4.20V
Ultralife	UBP001	1.80Ah*	1C	3.00V	4.20V

Table S2: **Additional cell testing information.** The table summarizes the nominal capacities (*indicates the re-rated capacity based on initial testing that deviated from the manufacturer rated capacity), the high C-Rate values ($C_{highrate}$) used during the diagnostic cycle, and the lower (V_{lower}) and upper (V_{upper}) voltage cutoffs employed during the diagnostic cycles.

Author Paper	Chemistry	Form Factor	Cell type	Temperature (°C)	SOC (%)	SOH at EOT (%)	Testing Duration
Keil et al. (2016) [1]	NCA/Gr	18650	Panasonic NCR18650PD	25	0	97.9	10 months
					5	97.4	10 months
					10	97.3	10 months
					20	96.7	10 months
					30	96.6	10 months
					40	96.6	10 months
					45	96.3	10 months
					50	96.3	10 months
					55	96.3	10 months
					60	94.4	10 months
					65	94.0	10 months
					70	93.8	10 months
					80	93.8	10 months
					90	93.5	10 months
					95	93.4	10 months
					100	93.2	10 months
				40	0	97.1	10 months
					5	95.9	10 months
					10	95.8	10 months
					20	94.8	10 months
					30	94.3	10 months
					40	94.0	10 months
					45	94.0	10 months
					50	93.9	10 months
					55	93.5	10 months
					60	92.2	10 months
					65	90.5	10 months
					70	90.3	10 months
					80	90.0	10 months
					90	89.4	10 months
					95	88.8	10 months
					100	88.7	10 months

				60	0	95.9	10 months
					5	94.4	10 months
					10	94.1	10 months
					20	92.8	10 months
					30	91.7	10 months
					40	91.6	10 months
					45	91.2	10 months
					50	91.2	10 months
					55	90.9	10 months
					60	89.7	10 months
					65	87.7	10 months
					70	87.2	10 months
					80	86.9	10 months
					90	86.3	10 months
					95	85.7	10 months
					100	84.8	10 months
	NMC/Gr	18650	Sanyo UR18650E	25	0	99.0	10 months
					5	98.6	10 months
					10	98.3	10 months
					20	98.0	10 months
					30	97.5	10 months
					40	97.5	10 months
					45	97.3	10 months
					50	97.4	10 months
					55	97.3	10 months
					60	97.1	10 months
					65	95.8	10 months
					70	94.7	10 months
					80	94.7	10 months
					90	94.5	10 months
					95	94.2	10 months
					100	93.5	10 months
				40	0	98.2	10 months
					5	97.2	10 months

					10	96.5	10 months
					20	95.6	10 months
					30	94.3	10 months
					40	93.8	10 months
					45	93.6	10 months
					50	93.5	10 months
					55	93.5	10 months
					60	93.3	10 months
					65	92.4	10 months
					70	90.0	10 months
					80	89.1	10 months
					90	89.0	10 months
					95	89.7	10 months
					100	81.5	10 months
				60	0	97.4	10 months
					5	95.4	10 months
					10	94.0	10 months
					30	90.1	10 months
					40	88.7	10 months
					50	88.0	10 months
					60	87.7	10 months
					65	87.7	10 months
					70	85.7	10 months
					80	82.7	10 months
					95	82.8	10 months
					100	76.7	10 months
LFP/Gr	18650	A123 APR18650M1A		25	0	100.0	10 months
					5	99.3	10 months
					10	98.5	10 months
					20	97.9	10 months
					30	97.2	10 months
					40	96.9	10 months
					45	97.2	10 months
					50	97.2	10 months
					55	97.2	10 months
					60	96.9	10 months
					65	96.5	10 months
					70	96.6	10 months

					80	94.1	10 months
					90	94.2	10 months
					95	94.4	10 months
					100	94.2	10 months
				45	0	97.8	10 months
					5	96.3	10 months
					10	95.2	10 months
					20	94.4	10 months
					30	93.8	10 months
					40	92.9	10 months
					45	92.5	10 months
					50	93.3	10 months
					55	92.7	10 months
					60	92.8	10 months
					65	92.8	10 months
					70	92.3	10 months
					80	90.3	10 months
					90	89.5	10 months
					95	89.9	10 months
					100	90.5	10 months
				60	5	92.6	10 months
					10	92.0	10 months
					20	91.2	10 months
					30	89.9	10 months
					40	88.4	10 months
					50	88.3	10 months
					55	88.2	10 months
					60	88.4	10 months
					65	88.0	10 months
					70	88.5	10 months
					80	86.6	10 months
					90	86.0	10 months
					95	85.7	10 months
					100	85.3	10 months
Naumann et al. (2018) [2]	LFP/Gr	26650	Sony Murata US26650FTC1	0	50	95.5	855 days
				10	50	95.3	855 days
				25	0	96.2	855 days
					50	93.7	855 days

					100	87.8	855 days
				40	0	94.8	855 days
					50	89.4	855 days
					100	85.3	855 days
				60	0	87.3	855 days
					50	79.2	855 days
					100	76.9	855 days
Frie et al. (2024) [3]	NCA/Si+Gr	18650	Samsung INR18650-35E	35	25	86.5	5 years
					28	85.8	5 years
					45	83.9	5 years
					59	83.7	5 years
					80	69.4	5 years
				40	25	86.0	5 years
					28	83.4	5 years
					45	80.4	5 years
					59	79.7	5 years
					80	68.1	5 years
				45	25	83.4	5 years
					28	83.2	5 years
					45	79.0	5 years
					59	78.0	5 years
					80	62.2	5 years
				50	25	74.8	5 years
					28	75.5	5 years
					45	74.4	5 years
					59	72.0	5 years
					80	60.9	5 years
Sarasketa-Zabala et al. (2014) [4]	LFP/Gr	26650	Unknown but commercially available	30	70	93.0	634 days
				40	30	90.7	593 days
					70	88.4	615 days
					90	88.6	350 days
				50	70	77.7	617 days
					90	84.0	291 days
Geisbauer et al. (2021) [5]	LFP/Gr	unknown	Heter Unknown	18.5	2	99.8	150 days
				50	2	96.1	150 days
					38	94.0	150 days
					100	86.4	150 days
				60	2	95.0	150 days

					38	93.1	150 days
					100	80.9	150 days
	NCA/Gr	unknown	Samsung Unknown	18.5	2	98.0	150 days
				50	2	92.6	150 days
					38	90.6	150 days
					100	85.5	150 days
				60	2	93.2	150 days
					38	91.2	150 days
					100	69.1	150 days
	NMC/Gr	unknown	Samsung Unknown	18.5	2	99.8	150 days
				50	2	93.6	150 days
					38	92.6	150 days
					100	77.5	150 days
				60	2	96.2	150 days
					38	94.2	150 days
					100	69.1	150 days
	LCO/Gr	unknown	Panasonic Unknown	18.5	2	99.8	150 days
				50	2	95.0	150 days
					38	93.5	150 days
					100	84.3	150 days
				60	2	94.1	150 days
					38	93.0	150 days
					100	77.9	150 days
	LCO/LTO	unknown	LTOBATTERY Co. Unknown	18.5	2	99.8	150 days
				50	2	99.0	150 days
					38	81.1	150 days
					100	86.2	150 days
				60	2	96.0	150 days
					38	73.8	150 days
					100	73.8	150 days
	LMO/Gr	unknown	Nitecore Unknown	18.5	2	101.0	150 days
				50	2	96.8	150 days
					38	95.4	150 days
					100	93.4	150 days
				60	2	97.9	150 days
					38	98.1	150 days
					100	88.9	150 days
Matadi et al. (2015) [6]	NMC/Gr	Pouch	Unknown	5	50	98.6	19 months

					90	98.4	19 months
					100	97.3	19 months
				25	50	97.6	21 months
					90	94.4	21 months
					100	93.5	21 months
				45	50	90.5	19 months
					90	83.7	20 months
					100	68.3	21 months
				60	50	84.3	12 months
					90	74.2	7 months
					100	70.0	4 months
Liu et al. (2020) [7]	NCA/Gr	18650	Panasonic NCR18650BD	10	20	93.7	435 days
					50	94.5	435 days
					90	92.1	435 days
				25	20	94.4	435 days
					50	95.5	435 days
					90	93.4	435 days
				45	20	94.4	435 days
					50	92.6	435 days
					90	89.7	435 days
Lucu et al. (2020) [8]	NMC442/Gr	Pouch	Unknown	25	50	102.4	600 days
					80	99.2	600 days
				35	20	103.3	569 days
					35	101.7	569 days
					50	101.5	569 days
					65	99.8	600 days
					80	96.3	600 days
					100	87.3	600 days
				45	50	97.5	481 days
					80	86.4	573 days
Werner et al. (2021) [9]	LCO+NCA/Gr	Pouch	Kokam Co., Ltd Unknown	40	35	90.6	102 weeks
					50	90.1	102 weeks
					65	89.8	102 weeks
					80	89.0	102 weeks
					100	84.2	102 weeks
				50	35	86.4	90 weeks
					50	85.4	90 weeks
					65	85.1	90 weeks

					80	83.8	90 weeks
					100	78.8	90 weeks
				60	35	88.1	26 weeks
					50	87.1	26 weeks
					65	86.9	26 weeks
					80	86.6	26 weeks
					100	81.5	26 weeks
Uddin et al. (2017) [10]	NCA/Gr	18650	Unknown	10	20	82.7	385 days
					50	82.7	385 days
					90	76.7	385 days
				25	20	85.8	385 days
					50	84.3	385 days
					90	80.6	385 days
				45	20	79.7	385 days
					50	77.7	385 days
					90	73.0	385 days
Wildfeuer et al. (2023) [11]	NCA/Si+Gr	18650	Sony/Murata US18650VTC5A	20	10	94.0	672 days
					50	91.2	672 days
					70	89.5	672 days
					100	89.2	672 days
				35	10	92.9	672 days
					50	87.8	672 days
					70	87.2	672 days
					100	85.3	672 days
				50	0	91.4	672 days
					10	89.6	672 days
					30	83.7	672 days
					40	82.6	672 days
					50	80.4	672 days
					55	80.4	672 days
					60	80.4	672 days
					65	80.2	672 days
					70	79.9	672 days
					75	79.6	672 days
					80	78.0	672 days
					85	76.4	672 days
					90	77.8	672 days
					95	78.0	672 days

					100	79.2	505 days
					100	79.2	505 days
				60	10	85.8	672 days
					50	73.5	672 days
					70	74.8	550 days
					100	90.4	83 days
Schmitt et al. (2017) [12]	NMC/Gr	18650	Sony US18650V3	0	50	97.2	469 days
					100	96.3	469 days
				20	25	96.8	470 days
					50	96.7	476 days
					75	94.3	476 days
					100	95.5	476 days
				45	50	92.0	467 days
					100	87.5	464 days
Zülke et al. (2021) [13]	NCA/Si+Gr	21700	Unknown/Can't be disclosed	25	0	98.1	12 months
					20	97.5	12 months
					40	96.4	12 months
					60	96.4	12 months
					70	94.9	12 months
					80	94.6	12 months
					90	95.6	12 months
					100	96.8	12 months
				40	0	97.7	12 months
					20	96.4	12 months
					40	94.1	12 months
					60	93.9	12 months
					70	92.4	12 months
					80	92.3	12 months
					90	93.6	12 months
					100	94.4	12 months
				50	0	97.5	12 months
					20	95.1	12 months
					40	91.8	12 months
					60	91.2	12 months
					70	90.3	12 months
					80	90.0	12 months
					90	91.2	12 months
					100	92.4	12 months

Dubarry and Devie (2018) [14]	(NCA+LCO)/LTO	Pouch Cells	Altairnano Generation 1	-27	5	98.9	66 weeks
					99	98.7	66 weeks
				25	50	99.8	66 weeks
					100	100.1	66 weeks
				45	20	96.6	66 weeks
					70	99.1	66 weeks
				55	5	85.8	66 weeks
					81.5	96.6	66 weeks
Schmalstieg et al. (2014) [15]	NMC/Gr	18650	Sanyo UR18650E	50	0	93.6	513 days
					10	90.5	513 days
					20	94.9	161 days
					30	81.8	514 days
					50	81.7	514 days
					60	90.5	161 days
					70	77.3	519 days
					80	76.1	405 days
					85	74.8	407 days
					90	75.4	346 days
					95	74.5	347 days
Redondo-Iglesias et al. (2017) [16]	LFP/Gr	Unknown	A123 Unknown	30	30	95.8	796 days
					65	94.1	796 days
					100	90.5	830 days
				45	30	84.9	704 days
					65	77.9	702 days
					100	79.5	700 days
				60	30	80.4	243 days
					65	57.4	517 days
					100	61.6	513 days
Schimpe et al. (2018) [17]	LFP/Gr	26650	Sony US26650FTC1	10	100	96.3	234 days
				15	0	99.6	234 days
					12.5	99.1	234 days
					25	98.6	234 days
					37.5	98.5	234 days
					50	98.4	234 days
					62.5	98.2	234 days
					75	97.4	234 days
					87.5	96.2	234 days
					100	96.3	234 days

				25	100	95.4	234 days
				35	100	94.2	234 days
				45	0	98.4	234 days
					12.5	96.5	234 days
					25	95.6	234 days
					25	95.6	234 days
					37.5	94.6	234 days
					50	94.4	234 days
					62.5	94.3	234 days
					75	93.7	234 days
					87.5	91.8	234 days
					100	92.0	234 days
Hahn et al. (2018) [18]	NMC111/Gr	Pouch Cell	Litec Battery GmbH HEA50	55	100	93.0	93 days
				40	85	91.3	270 days
				42.5	85	90.4	270 days
				45	85	89.4	270 days
				47.5	85	89.1	270 days
				50	0	96.2	270 days
				50	15	92.5	270 days
				50	22	88.5	270 days
				50	30	89.6	270 days
				50	40	83.0	270 days
				50	55	88.4	270 days
				50	70	88.6	270 days
				50	85	88.2	270 days
				50	90	86.6	270 days
				50	95	81.1	270 days
				50	100	80.2	270 days
				52.5	85	86.4	270 days
				55	55	86.0	270 days
				55	85	81.5	270 days
				60	85	76.1	270 days
Sui et al. (2021) [19]	LFP/Gr	cylindrical	unknown	40	50	82.6	43 months
				47.5	50	66.1	43 months
				55	10	77.6	27 months
					50	49.3	43 months
					90	69.3	27 months
Ecker et al. (2014) [20]	NMC/Gr	18650	Sanyo UR18650E	35	50	95.3	345 days

				40	50	92.8	344 days
				50	0	95.3	417 days
					10	93.1	418 days
					20	96.2	107 days
					30	85.1	407 days
					50	84.5	407 days
					60	92.4	107 days
					70	80.2	417 days
					80	76.2	419 days
					85	74.8	417 days
					90	75.4	357 days
					95	74.5	352 days
					100	54.9	157 days
Taniguchi et al. (2019) [21]	LCO/Gr	18650	Panasonic CGR18650E	80	0	99.0	143 days
					25	94.5	58 days
					50	94.3	19 days
					75	96.9	13 days
					100	56.3	7 days
Sun et al. (2021) [22]	Ni-rich/Gr	21700	Unknown	70	20	95.7	30 days
					60	93.6	22 days
					100	98.2	4 days
Wu et al. (2024) [23]	NMC811/Gr	Prismatic	CATL Unknown	25	100	97.9	183 days
				45	100	96.4	197 days
				60	100	94.2	183 days
				65	100	94.5	98 days
				75	100	95.9	35 days
Gewald et al. (2019) [24]	NMC/Gr	18650	Sony-Murata US18650VC7	25	60	95.4	382 days
				40	60	89.1	367 days
				60	60	79.3	382 days
				70	60	81.6	105 days
				80	60	90.0	19 days
Ecker et al. (2012) [25]	NMC/Gr	Pouch	Unknown	35	50	92.9	61 weeks
				50	50	89.8	61 weeks
				65	50	73.6	61 weeks
Du et al. (2021) [26]	Ni-based/Gr	18650	Unknown	80	100	87.4	45 days
Ishikawa et al. (2012) [27]	LCO/Gr	18650	Panasonic CGR18650E	70	87	91.5	28 days
				80	87	93.6	6 days
				90	87	93.8	1.4 days

100	87	96.1	.3 days

References

[1] Keil, P., Schuster, S.F., Wilhelm, J., Travi, J., Hauser, A., Karl, R.C., Jossen, A., (2016) Calendar aging of lithium-ion batteries. J. Electrochem. Soc., 163, A1872-A1880

[2] Naumann, M., Schimpe, M., Keil, P., Hesse, H.C., Jossen, A., (2018) Analysis and modeling of calendar aging of a commercial $LiFePO_4$ graphite cell. J. Energy Storage 17, 153-169

[3] Frie, F., Ditler, H., Klick, S., Stahl, G., Rahe, C., Ghaddar, T., Sauer, D.U., (2024) An Analysis of Calendaric Aging over 5 Years of Ni-rich 18650-Cells with Si/C Anodes. ChemElectroChem 202400020,

[4] Sarasketa-Zabala, E., Gandiaga, I., Rodriguez-Martinez, L.M., Villarreal, I., (2014) Calendar ageing analysis of a $LiFePO_4$ graphite cell with dynamic model validations: Towards realistic lifetime predictions. J. Power Sources 272, 45-57

[5] Geisbauer, C., W¨ohrl, K., Koch, D., Wilhelm, G., Schneider, G., Schweiger, H., Jossen, A., (2021) Comparative study on the calendar aging behavior of six different lithium-ion cell chemistries in terms of parameter variation. Energies 14, 3358

[6] Matadi, B.P., Geniès, S., Delaille, A., Waldmann, T., Kasper, M., Wohlfahrt-Mehrens, M., Aguesse, F., Bekaert, E., Jiménez-Gordon, E., Daniel, L., Fleury, X., Bardet, M., Martin, J., Bultel, Y., (2017) Effects of Biphenyl Polymerization on Lithium Deposition in Commercial Graphite/NMC Lithium-Ion Pouch-Cells during Calendar Aging at High Temperature. Journal of The Electrochemical Society 164, A1089-A1097

[7] Liu, K., Li, Y., Hu, X., Lucu, M., Widanage, W.D., (2023) Gaussian process regression with automatic relevance determination kernel for calendar aging prediction of lithium-ion batteries. IEEE Transactions on Industrial Informatics 16, 3767-3777

[8] Lucu, M., Martinez-Laserna, E., Gandiaga, I., Liu, K., Camblong, H., Widanage, W.D., Marco, J., (2020) Data-driven nonparametric Li-ion battery ageing model aiming at learning from real operation data – Part A: Storage operation. Journal of Energy Storage 30, 101409

[9] Werner, D., Paarmann, S., Wetzel, T., (2021) Calendar aging of li-ion cells—experimental investigation and empirical correlation. Batteries 7,

[10] Uddin, K., Jackson, T., Widanage, D.W., Chouchelamane, G., Jennings, P.A., Marco, J., (2017) On the possibility of extending the lifetime of lithium-ion batteries through optimal V2G facilitated by an integrated vehicle and smart-grid system. Energy 133, 710-722

[11] Wildfeur, L., Karger, A., Aygül, D., Wassiliadis, N., Jossen, A., Lienkamp, M., (2017) Experimental degradation study of a commercial lithium-ion battery Journal of Power Sources 560,

[12] Schmitt, J., Maheshwari, A., Heck, M., Lux, S., Vetter, M., (2017) Impedance change and capacity fade of lithium nickel manganese cobalt oxide-based batteries during calendar aging Journal of Power Sources 353

[13] Zülke, A., Yi, L., Keil, P., Burrell, R., Belaisch, S., Nagarathinam, M., Mercer, M., Hoster, H., (2021) High-Energy Nickel-Cobalt-Aluminium Oxide (NCA) Cells on Idle: Anode-versus Cathode-Driven Side Reactions Batteries & Supercaps Articles 4, 934-947

[14] Dubarry, M., Devie, A., (2018) Battery durability and reliability under electric utility grid operations: Representative usage aging and calendar aging J. Energy Storage 18, 185-195

[15] Schmalstieg, J., Käbitz, S., Ecker, M., Sauer, D.U., (2014) A holistic aging model for Li(NiMnCo)O2 based 18650 lithium-ion batteries. Journal of Power Sources 257, 325-334

[16] Redondo-Iglesias, E., Venet, P., Pelissier, S., (2017) Eyring acceleration model for predicting calendar ageing of lithium-ion batteries. Journal of Energy Storage 13, 176-186

[17] Schimpe, M., von Kuepach, M.E., Naumann, M., Hesse, H.C., Smith, K., Jossen, A., (2018) Comprehensive Modeling of Temperature-Dependent Degradation Mechanisms in Lithium Iron Phosphate Batteries. J. Electrochem. Soc. 165, A181–A193,

[18] Hahn, S.L., Storch, M., Swaminathan, R., Obry, B., Bandlow, J., Birke, K.P., (2018) Quantitative validation of calendar aging models for lithium-ion batteries. J. Power Sources 400, 402-414

[19] Sui, X., Świerczyński, M., Teodorescu, R., Stroe, D., (2021) The Degradation Behavior of LiFePO4/C Batteries during Long-Term Calendar Aging Energies 14

[20] Ecker, M., Nieto, N., Kabitz, S., Schmalstieg, J., Blanke, H., Warnecke, A., Sauer, D.U., (2014) Calendar and cycle life study of Li(NiMnCo)O_2 based 18650 lithium-ion batteries J. Power Sources 248, 839-851

[21] Taniguchi, S., Shironita, S., Konakawa, K., Mendoza-Hernandez, O.S., Sone, Y., Umeda, M., (2019) Thermal characteristics of 80°C storage-degraded 18650-type lithium-ion secondary cells J. Power Sources 416, 148-154

[22] Sun, Y., Zhang, S., Qi, J., Su, Z., (2021) Calendar degradation of Li-ion batteries under high storage temperature based on electrochemical impedance spectroscopy Microelectronics Reliability 126

[23] Wu, K., Wu, X., Lin, Z., Sun, H., Wang, M., Li, W., (2024) Identifying the calendar aging boundary and high temperature capacity fading mechanism of Li-ion battery with Ni-rich cathode. Journal of Power Sources 589, 233736

[24] Gewald, T., Candussio, A., Wildfeuer, L., Lehmkuhl, D., Hahn, A., Lienkamp, M., (2019) Accelerated aging characterization of lithium-ion cells: Using sensitivity analysis to identify the stress factors relevant to cyclic aging. Batteries 6,

[25] Ecker, M., Gerschler, J.B., Vogel, J., Käbitz, S., Hust, F., Dechent, P., Sauer, D.U. , (2012) Development of a lifetime prediction model for lithium-ion batteries based on extended accelerated aging test data. Journal of Power Sources 215, 248-257

[26] Du, Y., Fujita, K., Shironita, S., Sone, Y., Hosono, E., Asakura, D., Umeda, M. , (2021) Capacity fade characteristics of nickel-based lithium-ion secondary battery after calendar deterioration at 80 °C Journal of Power Sources 501, 230005

[27] Ishikawa, H., Mendoza, O., Sone, Y., Umeda, M. , (2021) Study of thermal deterioration of lithium-ion secondary cell using an accelerated rate calorimeter (ARC) and AC impedance method. Journal of Power Sources 198 236-242